RSC Advances

PAPER

View Article Online
View Journal | View Issue

Cite this: *RSC Adv.*, 2014, **4**, 7838

Optimal Ag_2S nanoparticle incorporated TiO_2 nanotube array for visible water splitting

Mostafa Gholami,[a] Mohammad Qorbani,[a] Omran Moradlou,[b] Naimeh Naseri[c] and Alireza Z. Moshfegh*[ad]

Received 5th September 2013
Accepted 20th November 2013

DOI: 10.1039/c3ra44898c

www.rsc.org/advances

Free-standing TiO_2 nanotube array (TNA) films were fabricated *via* two-step anodization of a titanium sheet. The X-ray diffraction pattern indicated amorphous TNAs were transformed into anatase after annealing the films at 500 °C in air. The surface of TNA was modified by a sequential-chemical bath deposition (S-CBD) method to fabricate Ag_2S nanoparticles and forming TNA/Ag_2S-*n* nanostructure, by varying the number of cycles (*n*). Based on SEM observations, the produced films consisted of vertically ordered tubular structure arrays, each with 125 nm in diameter and 4.1 μm in length containing silver sulphide nanoparticles of ~12 nm diameter. X-Ray photoelectron spectroscopy (XPS) confirmed the formation of Ag_2S nanoparticles on TNA film. Increased optical absorption of the TNA/Ag_2S system in visible and near infrared was also verified by diffuse reflectance spectroscopy (DRS). Maximum photocurrent density of about 840 μA cm^{-2} was measured for the synthesized TNA/Ag_2S-4 photoanode under visible irradiation which exhibited about 15 fold photo-enhancement in current density as compared with the pure TNAs under similar conditions. The incident photon to current efficiency (IPCE) measurements indicated that the visible response of the samples reached its maximum value of about 20% at a wavelength of 600 nm for the TNA/Ag_2S photoanode.

1. Introduction

Water splitting for H_2 generation using a photocatalytic material or a photoelectrochemical (PEC) cell with simultaneous solar radiation is a sustainable approach for producing a clean and renewable energy carrier. For the first time, Fujishima and Honda have discovered photochemical water splitting using TiO_2 photoelectrode irradiated by ultraviolet (UV) light.[1] Up to now, many investigations have been carried out to develop PEC water splitting performance of semiconductor photocatalysts such as TiO_2,[2] WO_3,[3] and ZnO.[4]

Currently, titanium dioxide has been extensively used for water splitting in photoelectrochemical cells due to its high PEC efficiency in energy conversion, chemical stability and low cost.[5,6] However, because of wide band gap energy (3.2 eV), TiO_2 is an active photocatalyst only in the UV region of the solar spectrum. Furthermore, the high recombination rate of photo-generated electron–hole pairs decreases the efficiency of pure TiO_2 based PEC cells.

Currently, several nanostructures of TiO_2, especially nanotubular structures, have been used to increase the surface to volume ratio.[7,8] Besides, it is well understood that the one-dimensional geometry of TiO_2 nanotube arrays (TNA) facilitates charge carrier transfer in the system.[8] To activate TNA photoanodes in visible light, a series of techniques have been used such as doping with other elements like N,[9] C,[10] S,[11] and Si (ref. 12) or coupling with narrow band gap semiconductors including WO_3,[13] ZnO,[14] CdS,[15] CdSe,[16] Cu_2O,[17] AgBr,[18] and CdS/CdSe.[19] Among low band gap semiconductors, silver sulfide (Ag_2S) is a suitable and promising material responding in the whole solar energy spectra with a direct band gap of about 1.0 eV.[20] Its conduction band (−0.3 eV) is less anodic than the corresponding TiO_2 band (−0.1 eV), and its valence band (+0.7 eV) is more cathodic than the TiO_2 valence band (+3.1 eV).[21] Ag_2S has been utilized as a competent material for photovoltaic cells,[22] infrared detectors,[23] electronic devices[24] and photocatalysis.[25–27] Nagasuna *et al.* have reported photoelectrochemical measurements of coupled TiO_2/Ag_2S system under simulated sunlight illumination.[26] Shen *et al.* has also studied the effect of Ag_2S loading on nanostructured CdS for photocatalytic hydrogen evolution.[28] They have found that the catalytic behavior of Ag_2S in hole transfer can enhance the H_2 production rate significantly. Recently, Xie *et al.* have applied Ag_2S quantum dots to sensitize TNAs in the visible range.[29] They have obtained the best photoresponse of about 120 μA cm^{-2} for an optimum surface loading of silver

[a]*Department of Physics, Sharif University of Technology, P.O. Box 11555-9161, Tehran, Iran. E-mail: moshfegh@sharif.edu*

[b]*Department of Chemistry, Faculty of Sciences, Alzahra University, P.O. Box: 1993893973, Tehran, Iran*

[c]*School of Physics, Institute for Research in Fundamental Sciences(IPM), P.O. Box: 1939-55531, Tehran, Iran*

[d]*Institute for Nanoscience and Nanotechnology, Sharif University of Technology, P.O. Box 14588-8969, Tehran, Iran*

sulfide quantum dots. Regardless of these few published reports on Ag_2S-modified TNA electrodes, different aspects of PEC performance such as wavelength dependence efficiency, electron lifetime, electrochemical impedance spectroscopy and charge transport resistance of TNA/Ag_2S system have not yet been completely studied.

In this study, a coupled TNA/Ag_2S system has been synthesized and their photocatalytic activity for a water splitting reaction has been investigated. The surface morphology has been monitored using field emission scanning electron microscopy (FE-SEM). The optical properties, crystalline structure and surface chemical composition of the samples have been studied using UV-visible diffuse reflectance spectroscopy (DRS), X-ray diffractometry (XRD), and X-ray photoelectron spectroscopy (XPS), respectively. Finally, the photoelectrochemical (PEC) properties of the coupled TNA/Ag_2S system have been extensively studied under visible irradiation. The results of the incident photon to current conversion efficiency (IPCE), open circuit photovoltage (V_{oc}) and electrochemical impedance spectroscopy have also been presented for the first time.

2. Experimental

2.1. Samples preparation

Free-standing TiO_2 nanotube array films were fabricated *via* two-step anodization of titanium (Ti) sheet (99.5% purity, 0.5 mm thickness). The electrolyte consisted of de-ionized (DI) water and ethylene glycol (99.9%, Merck) solution with the volume ratio of 10 : 90, containing 0.5 M NH_4F (Merck). Then, a few drops of 1 M H_3PO_4 aqueous solution were added to adjust the pH to 5.7. The anodization process was performed at an optimized applied voltage of 60 V for a total time of 200 min. In the first step, the Ti sheet was anodized for 50 min and then 150 min for the second step. The samples were sonicated for 40 s between these two steps. Then, to crystallize the grown structures; they were annealed in air at 500 °C for 80 min with a heating rate of about 10 °C min^{-1} as reported by others.[30]

Surface modification of TNA was performed by using a sequential-chemical bath deposition (S-CBD) method to fabricate Ag_2S nanoparticles on the produced TNA surface. TNA/Ag_2S photoanodes were synthesized following Tubtimtae *et al.*'s work.[31] In this method, 0.1 M ethanolic $AgNO_3$ (pH ~ 7) solution was prepared by adding a suitable amount of $AgNO_3$ to ethanol and stirring for 60 min. This solution was a cationic precursor in the S-CBD method. The TNA sample was immersed in this solution for 1 min. Then the sample was washed out by ethanol to remove loosely bound and excess precursor solution. Afterwards, the sample was immersed for 3 min in a 0.1 M Na_2S methanolic solution (as anionic precursor) to deposit Ag_2S nanoparticles. Then, the sample was washed with ethanol again. These sequential four steps, proceeding at room temperature, were considered as one cycle (Fig. 1(a)). Such a cycle was repeated several times, called number of cycles (n) to make a TNA/Ag_2S-n (n = 2, 3, 4, 5, 6 and 8) film. After each cycle, the appearance of the sample turned darker as can be seen in Fig. 1(b) and also other reports.[25,28]

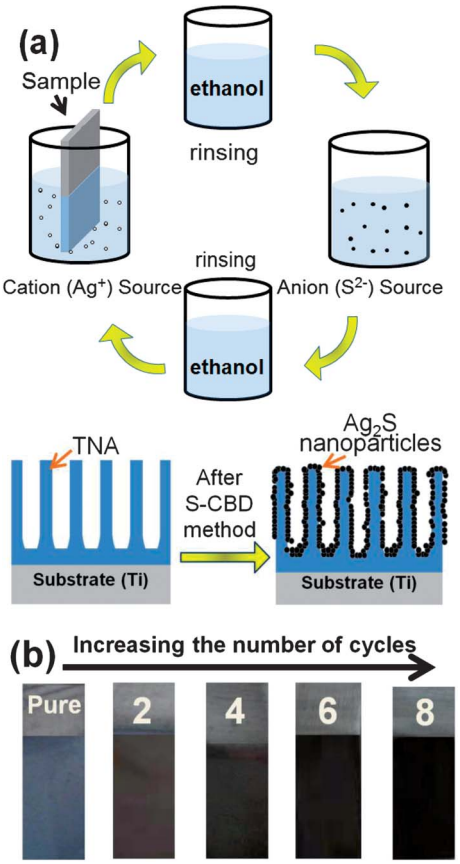

Fig. 1 (a) Schematic of S-CBD process in each cycle for depositing Ag_2S nanoparicles and (b) the observed changes in the sample's color by increasing the cycle number.

2.2. Physical and photoelectrochemical characterization

The morphology of the annealed samples was monitored by FE-SEM (Hitachi-s-4160). The crystalline structure was detected and identified by the XRD technique with radiation of a Cu target (K_α, λ = 0.154 nm). The surface chemical state of the coupled TNA/Ag_2S nanostructures was examined by XPS using a monochromated Al Kα radiation source (1486.6 eV) at a pressure lower than 10^{-7} Pa. For the analysis of XPS data, SDP (version 4.1) software was used in this study. Moreover, the optical properties of the prepared samples were investigated by DRS technique.

PEC properties of the prepared photoanodes (coupled TNA/Ag_2S-n system) were investigated in a three-electrode cell by galvanostat/potentiostat electroanalyzer (Autolab PGSTAT302). The photoanodes, Pt wire and Ag/AgCl have been used as working, counter and reference electrodes, respectively. The photoanode was suspended into 0.5 M Na_2S solution, and exposed to 300 W Xe-lamp with power density of about 25 mW cm^{-2}. A UV cut off filter (λ < 395 nm) was placed between the source and the sample to assure applying visible light irradiation. The photocurrent generated from the photoanode was recorded according to the responses to sudden switching on and off (at a constant bias voltage of 0 V *vs.* Ag/AgCl electrode). The incident photon to current efficiency (IPCE) and open

circuit voltage (V_{oc}) of the samples were also investigated. In order to perform IPCE measurements for different samples at each wavelength, the light source was equipped with a monochromator.

3. Results and discussion

3.1. Physical characterizations

Fig. 2 shows FE-SEM images of the pure and Ag_2S loaded TNA samples. According to Fig. 2(a), the average size of the inner diameter and the wall thickness of pure TNAs were measured as about 125 and 30 nm, respectively. Moreover, based on observation of cross view images, the average length of the nanotubes was obtained as 4.1 μm. As depicted in Fig. 2, the nanotubes are clearly formed in ordered manner and arranged with highly oriented morphology. The FE-SEM images of TNA/Ag_2S-n samples are shown in Fig. 2(b)–(d) for $n = 2$, 4 and 6, respectively. It can be clearly seen that in all samples, Ag_2S nanoparticles have been formed on the top and lateral side of the TNAs confirming successful surface deposition of silver sulfide without damaging the TiO_2 nanotube architectures. In addition, from SEM cross views, it is obvious that the size of Ag_2S nanoparticles increased with increasing number of deposition cycles (n). By averaging the size of Ag_2S nanoparticles in Fig. 2(c), we have obtained $d \sim 12$ nm for the TNA/Ag_2S-4 sample. Furthermore, according to top view SEM image analysis, by increasing the number of cycles, surface accumulation of Ag_2S nanoparticles increased that may cover (block) some tube mouths (see for example Fig. 2(d)).

The recorded XRD pattern of the synthesized pure TNA sample is shown in Fig. 3. The main observed diffraction peak of TiO_2 occurs at $2\theta = 25.3^\circ$ which is attributed to (101) orientation and represents the formation of the anatase crystalline phase in annealed films. Additionally, the Ti peaks in this system come from the substrate.

By applying Scherrer's equation, $D = 0.9\lambda/(\beta \cos \theta)$, where λ is the wavelength of the incident X-ray radiation, β is the full-width at half-maximum (FWHM) of the desired peak in radians and θ is the Bragg angle, the average size of TiO_2 nanocrystals was estimated about 30 nm for the main peak.[32]

We also performed X-ray diffraction analysis of the TNA/Ag_2S system, but due to the small Ag_2S particle size we could not obtain a reliable and clear XRD spectrum for this sample. In this regard, X-ray photoelectron spectroscopy (XPS) was used for detecting Ag_2S nanoparticles.

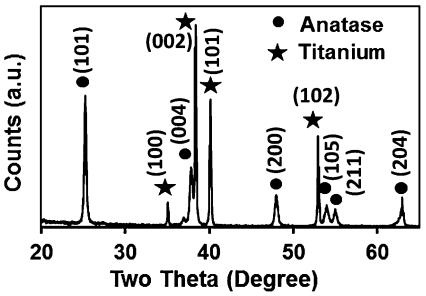

Fig. 3 XRD pattern of the annealed TNA sample.

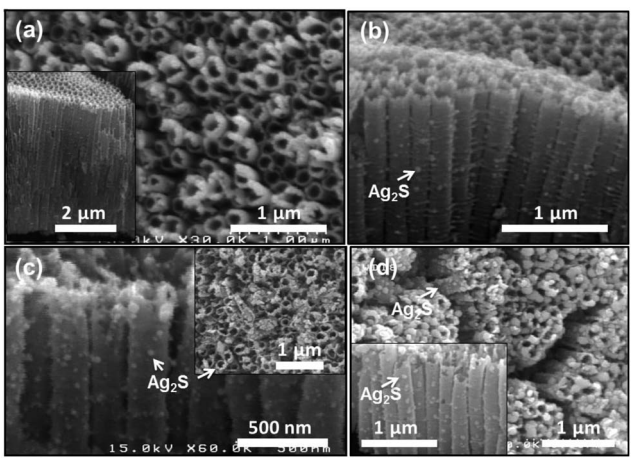

Fig. 2 FE-SEM images of different photoanodes: (a) TNA, (b) TNA/Ag_2S-2, (c) TNA/Ag_2S-4 and (d) TNA/Ag_2S-6.

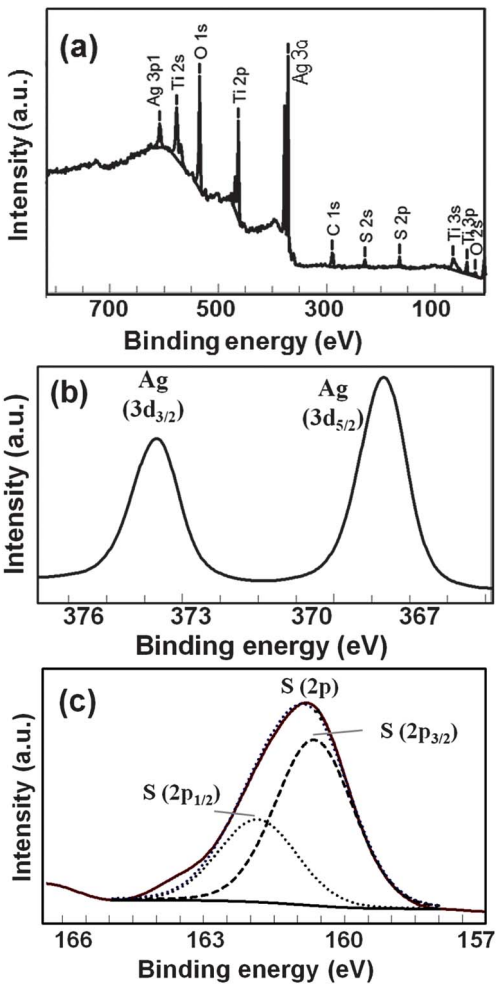

Fig. 4 (a) XPS survey spectrum of the TNA/Ag_2S-4 sample, and high resolution spectra in (b) Ag(3d) and (c) S(2p) core level.

The XPS survey spectrum of the coupled TNA/Ag_2S-4 system (Fig. 4(a)) indicated the existence of Ti, O, Ag and S elements on the samples. A trace amount of carbon was also observed in the survey as a result of surface adsorbed pollutions/contaminations (such as CO/CO_2) in air. Based on high resolution XPS spectra analysis of the Ti(2p) and O(1s) core level peaks (not shown), we have found that the O/Ti ratio is about 2.0 ± 0.05 which confirmed a stoichiometric formation of titanium dioxide in the films.

Fig. 4(b) and (c) show high resolution XPS spectra of Ag(3d) and S(2p) core level peaks, respectively. The Ag(3d) spectrum contains two peaks—one at 367.4 eV for the Ag($3d_{5/2}$) and the other at 373.4 eV for the Ag($3d_{3/2}$), which are in good agreement with the published values of the Ag(3d) signal in Ag_2S compound.[33,34] The S(2p) peaks were also deconvoluted into two separate peaks: one at 161.0 eV for the S($2p_{3/2}$) and another at 162.2 eV for the S($2p_{1/2}$) peak due to the split orbiting theory.[33,34] After analysis of the area surrounded by each peak, the atomic surface concentrations of Ag and S were determined at about 13.7 and 4.7%, respectively. This means that the synthesized Ag_2S nanoparticles were Ag rich. This richness of cation by S-CBD deposition method has also been observed recently for the growth of CdS nanoparticles.[35] Further XPS analysis of the sample resulted in surface ratios of Ag : Ti and S : Ti of about 0.89 and 0.31, respectively. To the best of our knowledge, XPS analysis of fabricated Ag_2S nanoparticles by S-CBD method has not been published yet.

Fig. 5 illustrates UV-visible absorption spectra of the TNA/Ag_2S-n samples with various S-CBD cycle numbers. According to data analysis, the absorption edge for a pure TNA sample occurred at about 380 nm. This result is in agreement with the band gap energy (E_g = 3.2 eV) of TiO_2 in the anatase phase.[36] The optical absorption of the samples in the visible range increased with increasing the deposition process cycles (n), which confirms higher loadings of visible active Ag_2S nanoparticles on the surface, as also observed and verified in the corresponding SEM images (see Fig. 2). Results similar to these are reported in other works.[29,31]

3.2. PEC Measurements

3.2.1. Photoresponsivity. In order to investigate the electrochemical behavior of the fabricated photoanodes and to select an appropriate bias voltage, cyclic voltammetry (CV) under dark and illumination conditions was applied in the range of −0.6 to 0.6 V using 0.5 M Na_2S solution as the supporting electrolyte. In the measured CV curves corresponding to pure TNA and TNA–Ag_2S samples (not shown here), no oxidation or reduction peaks were observed which indicated photoelectrochemical stability of all samples.

Fig. 6 illustrates the photoresponse of different TNA/Ag_2S-n electrodes under visible irradiation as compared with pure TNA electrode in chopping the light source. All experiments were carried out under ~25 mW cm^{-2} power intensity, at 0 V bias and 0.5 M aqueous solution of Na_2S as electrolyte. The results show that upon illuminating the photoanode surface, a significant photocurrent was generated for all samples indicating high photo activity with a durable photoresponse in time. However, based on the results, a photocurrent density of TNA/Ag_2S-n photoanodes was obtained of 290, 395, 840, 535, 385 and 206 μA cm^{-2} for samples with n = 2, 3, 4, 5, 6 and 8 cycles, respectively. These values were much higher than that for pure TNA photoanode (56 μA cm^{-2}). The highest photoresponse was observed for the TNA/Ag_2S-4 sample, which was about 15 times higher than the photocurrent obtained for pure TNA under similar conditions.

Fig. 7(a) shows the measured photocurrent density for TNA/Ag_2S-4 as a function of applied bias voltages ranging from 0 to 1 V (at different illumination intensities). The photocurrent of the TNA/Ag_2S-4 sample increased with the incident light intensity as also measured for the Au : TiO_2 nanocomposite system by our group.[37]

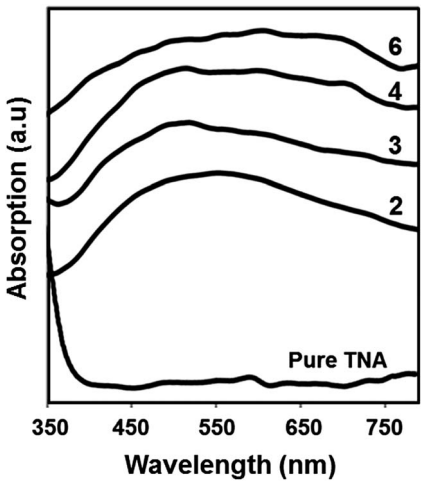

Fig. 5 UV-visible absorption spectra of the pure TNA (n = 0) and the TNA/Ag_2S-n different cycles (n).

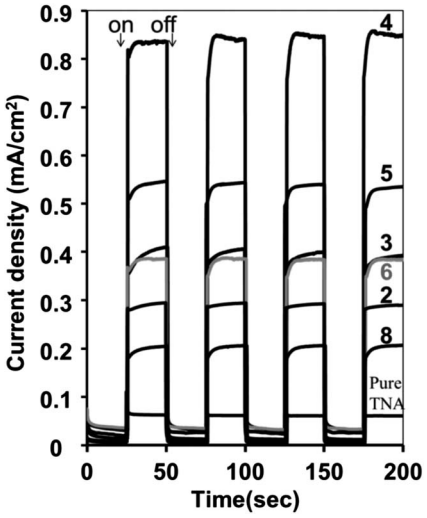

Fig. 6 Photocurrent density response of pure TNA and different TNA/Ag_2S-n samples.

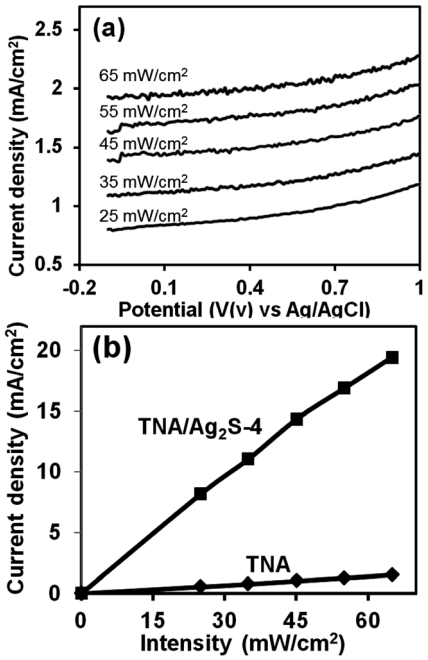

Fig. 7 Photocurrent density of the TNA/Ag_2S-4, *versus* (a) applied potential and (b) illuminating light intensity at 0 V bias.

In order to understand the relationship between the generated photocurrent density (J_{ph}) and the applied illumination intensity (I_{light}), a diagram of J_{Ph} *versus* I_{light} was drawn at 0 V potential (Fig. 7(b)). A linear relation between J_{ph} and I_{light} was found indicating that the charge carriers (e^-–h^+ pair) generation is a dominant phenomenon in the water splitting reaction.[38] Similar results have been also obtained for other samples.

To study the incident photon to current conversion efficiency (IPCE) at different wavelengths, experiments were performed in a PEC cell at 0 V bias under illumination from 370 to 700 nm wavelength. IPCE of the prepared photoelectrodes was measured using the following relation:

$$\mathrm{IPCE} = 1240 J_{Ph}(\mathrm{mA\ cm^{-2}})/[\lambda(\mathrm{nm}) P(\mathrm{W\ cm^{-2}})] \quad (1)$$

where λ is the wavelength of the incident photon, J_{ph} and P are photocurrent density and the intensity of illuminating light at each wavelength, respectively. Fig. 8 illustrates the obtained IPCE (%) of the photoelectrodes as a function of the wavelength. The highest IPCE value of pure TNA photoelectrode was found as 50% at $\lambda = 370$ nm and it was negligible for wavelengths greater than 400 nm. However, after deposition of Ag_2S nanoparticles, the IPCE values significantly increased in the visible region. However, IPCE values decreased in the UV region due to higher loading of Ag_2S nanoparticles on the surface (as also supported by our SEM observation), as a result of limited interaction of incident light with UV active material (TiO_2). The highest visible response (~20%) was observed for the TNA/Ag_2S-4 photoelectrode at $\lambda \sim 600$ nm. Therefore, the photoresponsivity of Ag_2S nanoparticles is active in a larger wavelength domain as compared to other semiconductors such as CdS.

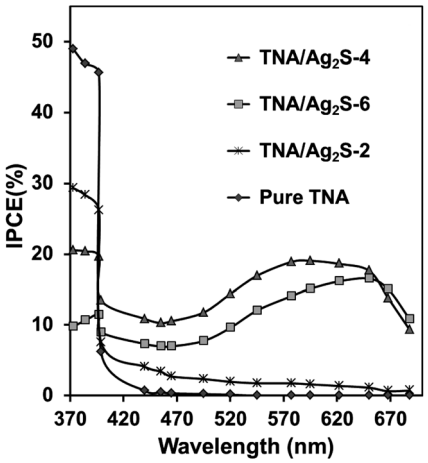

Fig. 8 IPCE of different photoanodes *versus* irradiated wavelength.

3.2.2. Transient time of charge carriers. By scanning the open circuit photovoltage (V_{oc}), the kinetics of the recombination process of the samples has been investigated. First, the samples were exposed to 25 mW cm^{-2} Xe lamp in sufficient time. When the light was turned off, the variation of V_{oc} was recorded as a function of time. A slow decay of V_{oc} indicated long lifetimes for photogenerated e^-–h^+ pair promising high photo activity of the films during the water splitting reaction. The lifetime of the photogenerated electrons in the sample in each energy state was calculated from the following formula.[39]

$$\tau_n = k_B T(\mathrm{d}V_{oc}/\mathrm{d}t)^{-1}/e \quad (2)$$

Here, k_BT, t, e and τ_n are thermal energy, time, elementary charge and lifetime in the dark condition, respectively. Fig. 9 shows the measured transient times of all samples in different energy states. According to the figure, with increase in the number of cycles up to $n = 4$, the transient time was increased in all energy states, while for samples with higher n values, the measured transient time was reduced. This result is in full agreement with the observed behavior in Fig. 6.

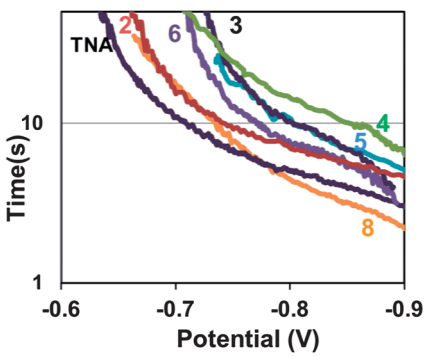

Fig. 9 Transient times in different energy states based on open circuit chronovoltammetry.

3.2.3. Electrochemical impedance spectroscopy. To investigate the electrical properties of the fabricated samples, electrochemical impedance spectroscopy was used. Fig. 10 represents the Nyquist (imaginary *versus* real part of resistance) plots of the TNA photoanodes with different amounts of Ag_2S loading, at a single constant potential (0 V) with 10 mV potential perturbation amplitude. The relevant equivalent circuit resulting in the best fittings was also inserted into the figure. R_1, R_2 and Q_1 were related to the ohmic resistances and capacitance of the cell (electrolyte and counter electrode). Q is a constant phase element, which is usually used instead of a pure capacitor for the oxide systems.[40] According to the literature, (R_3, Q_2) is attributed to the electron transport in the grains body.[41] The measured values for the charge transport resistance of the films are listed in Table 1. These obtained values are in agreement with the ones reported in the literature for TNA based photoanodes.[42]

It can be seen that by loading a small amount of Ag_2S nanoparticles on the TNA surface, the charge transport resistance of the samples increased to nearly two times. This result may attribute to wthe eak contact between small Ag_2S particles and a nanotube mouth. However, by increasing the cycle number, due to a more effective interface between Ag_2S nanoparticles and titanium nanotube, the resistance decreased significantly. The least value of R_{ct} was measured of about 3.2 kΩ for $n = 5$.

Using Mott–Schottky plots (not shown here) and related relation,[40,43] flat band potential of all samples was calculated as −0.6 V which was reasonable as compared with other reports.[43] Moreover, donor density of the samples was in the range of 2.7–12.2 × 10^{22} m^{-3} with a maximum value for films with $n = 5$.

To explain the reason for observing an optimum cycle number for Ag_2S deposition on TNA photoanodes ($n = 4$), all positive and negative aspects of silver sulfide role should be considered. First, according to DRS data, the addition of more Ag_2S to the surface increased the visible absorption of the samples and hence, improved the responses of the corresponding photoelectrodes. This phenomenon is mainly responsible for enhancement of the PEC performance of the samples by increasing n from 0 to 4. On the other hand, for $n \leq 4$, photogenerated electrons shift to the conduction band of TNAs causing separation of the charge carriers and increasing the lifetime duration of photoanodes. However, based on SEM results and related discussions, the bigger number of cycles results in a bigger size of nanoparticles. As a result of increasing the particle size and surface density, the mouth of TiO_2 nanotubes can be covered. This phenomenon is clear in IPCE measurements that show reduction of UV response. Hence, transfer of photogenerated electrons from Ag_2S particles to TNA and then, to the back contact will be harder. This negative effect of increasing the n value can be followed in V_{oc} decay kinetics (Fig. 9) and electrochemical impedance (Fig. 10) results. Nevertheless, in higher n values, electron–hole recombination is more probable due to a less effective connection between surface excited electrons and TNA channels. These two positive and negative sides of Ag_2S addition resulted in an optimum cycle number ($n = 4$) leading to the highest photoresponse density and IPCE value.

Table 1 Measured charge transport resistance of the synthesized TNA–Ag_2S photoanodes

Number of cycles (n)	0 (TNA)	2	3	4	5	6	8
R_{ct} (kΩ)	16.3	31.2	30.5	6.7	3.2	6.3	5.7

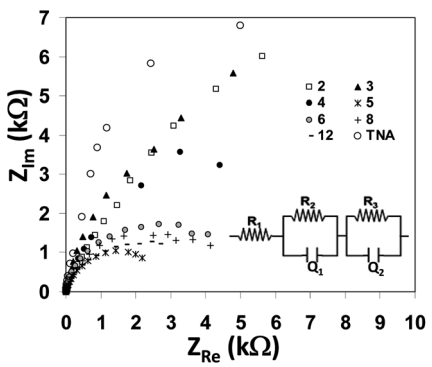

Fig. 10 Nyquist plots of the different TNA–Ag_2S photoanodes.

4. Conclusions

In this research, we have provided the TiO_2 nanotube arrays by using the anodization method. Afterwards, Ag_2S nanoparticles were deposited on the TNA by S-CBD process. The formed Ag_2S nanoparticles were shown in a SEM image, which were also confirmed by XPS analysis. Our results showed that TNAs were photoelectrochemically activated by Ag_2S nanoparticles. Optimizing the Ag_2S deposition cycles, the best photocurrent was obtained as 840 μA cm^{-2} (under 25 W m^{-2}) which was about 15 times higher than the one achieved for pure TNA. In fact, Ag_2S nanoparticles passivate the charge recombination centers and enhanced electron–hole separation. For the first time, we have reported IPCE (20% for the best one), open circuit photovoltage and charge transport resistance of the TNA/Ag_2S-n system.

Acknowledgements

The authors would like to thank the Research and Technology Council of Sharif University of Technology for financial support. The useful assistance of Mr S. Rafiee regarding XPS measurements is greatly acknowledged.

References

1 A. Fujishima and K. Honda, *Nature*, 1972, **238**, 37–38.
2 J. Li, C.-J. Lin, J.-T. Li and Z.-Q. Lin, *Thin Solid Films*, 2011, **519**, 5494–5502.
3 N. Naseri, R. Azimirad, O. Akhavan and A. Z. Moshfegh, *Thin Solid Films*, 2010, **518**, 2250–2257.

4 M. Liu, C. Y. Nam, C. T. Black, J. Kamcev and L. Zhang, *J. Phys. Chem. C*, 2013, **117**, 13396–13402.
5 C. A. Grimes and G. K. Mor, *TiO_2 Nanotube Arrays: Synthesis, Properties, and Applications*, Springer, New York, 2009.
6 J. Gong, Y. Lai and C. Lin, *Electrochim. Acta*, 2010, **55**, 4776–4782.
7 P. Roy, S. Berger and P. Schmuki, *J. Nanosci. Nanotechnol.*, 2011, **50**, 2904–2913.
8 A. Z. Moshfegh, *J. Phys. D: Appl. Phys.*, 2009, **42**, 233001–233031.
9 K. Shankar, K. C. Tep, G. K. Mor and C. A. Grimes, *J. Phys. D: Appl. Phys.*, 2009, **39**, 2361–2366.
10 J. H. Park, S. Kim and A. J. Bard, *Nano Lett.*, 2006, **6**, 24–28.
11 T. Umebayashi, T. Yamaki, H. Itoh and K. Asai, *Appl. Phys. Lett.*, 2002, **81**, 454–456.
12 Y. Su, S. Chen, X. Quan, H. Zhao and Y. Zhang, *Appl. Surf. Sci.*, 2008, **255**, 2167–2172.
13 A. Benoit, I. Paramasivam, Y. C. Nah, P. Roy and P. Schmuki, *Electrochem. Commun.*, 2009, **11**, 728–732.
14 Y. Yang, X. Wang, C. Sun and L. Li, *J. Appl. Phys.*, 2009, **105**, 094304.
15 M. Liu, J. Zheng, Q. Liu, S. Xu, M. Wu, Q. Xue, Z. Yan, H. Xiao, Z. Wei and H. Zhu, *RSC Adv.*, 2013, **3**, 9483–9489.
16 N. Guijarro, T. Lana-Villarreal, Q. Shen, T. Toyoda and R. Gómez, *J. Phys. Chem. C*, 2010, **114**, 21928–21937.
17 Z. Li, J. Liu, D. Wang, Y. Gao and J. Shen, *Int. J. Hydrogen Energy*, 2012, **37**, 6431–6437.
18 Q. Li, Y. Xing, R. Li, L. Zong, X. Wang and J. Yang, *RSC Adv.*, 2012, **2**, 9781–9785.
19 S. Huang, Q. Zhang, X. Huang, X. Guo, M. Deng, D. Li, Y. Luo, Q. Shen, T. Toyoda and Q. Meng, *Nanotechnology*, 2010, **21**, 375201.
20 Y. Xie, S. H. Heo, Y. N. Kim, S. H. Yoo and S. O. Cho, *Nanotechnology*, 2010, **21**, 015703.
21 M. C. Neves, J. M. F. Nogueira, T. Trindade, M. H. Mendonça, M. I. Pereira and O. C. Monteiro, *J. Photochem. Photobiol., A*, 2009, **204**, 168–173.
22 H. M. Pathan, P. V. Salunkhe, B. R. Sankapal and C. D. Lokhande, *Mater. Chem. Phys.*, 2001, **72**, 105–108.
23 Y. Du, B. Xu, T. Fu, M. Cai, F. Li, Y. Zhang and Q. Wang, *J. Am. Chem. Soc.*, 2010, **132**, 1470–1471.
24 W. Hailiang and Q. Limin, *Adv. Funct. Mater.*, 2008, **18**, 1249–1256.
25 C. Chen, Y. Xie, G. Ali, S. H. Yoo and S. O. Cho, *Nanoscale Res. Lett.*, 2011, **6**, 462–470.
26 K. Nagasuna, T. Akita, M. Fujishima and H. Tada, *Langmuir*, 2011, **27**, 7294–7300.
27 L. Zhu, Z. D. Meng and W. C. Oh, *J. Nanomater.*, 2012, **2012**, 586526.
28 S. Shen, L. Guo, X. Chen, F. Ren and S. S. Mao, *Int. J. Hydrogen Energy*, 2010, **35**, 7110–7115.
29 Y. Xie, S. H. Yoo, C. Chen and S. O. Cho, *Mater. Sci. Eng., B*, 2012, **177**, 106–111.
30 Y. Tian, C. Hu, X. He, C. Cao, G. Huang and K. Zhang, *Sens. Actuators, B*, 2010, **144**, 203–207.
31 A. Tubtimtae, K.-L. Wu, H.-Y. Tung, M.-W. Lee and G. J. Wang, *Electrochem. Commun.*, 2010, **12**, 1158–1160.
32 B. D. Cullity, *Elements of X-ray Diffraction*, Addison-Wesley, London, 1978, 2nd edn.
33 B. Subash, B. Krishnakumar, V. Pandiyan, M. Swaminathan and M. Shanthi, *Sep. Purif. Technol.*, 2012, **96**, 204–213.
34 F. Jia, Z. Yao and Z. Jiang, *Int. J. Hydrogen Energy*, 2012, **37**, 3048–3055.
35 C. J. Lin, Y. H. Yu and Y. H. Liou, *Appl. Catal., B*, 2009, **93**, 119–125.
36 R. Beranek, H. Tsuchiya, T. Sugishima, J. M. Macak, L. Taveira, S. Fujimoto, H. Kisch and P. Schmuki, *Appl. Phys. Lett.*, 2005, **87**, 243114–243117.
37 N. Naseri, P. Sangpour and A. Z. Moshfegh, *Electrochim. Acta*, 2011, **56**, 1150–1158.
38 M. A. Butler, *J. Appl. Phys.*, 1977, **48**, 1914–1921.
39 A. Zaban, M. Greenshtein and J. Bisquert, *ChemPhysChem*, 2003, **4**, 859–864.
40 A. J. Bard and L. R. Faulkner, *Electrochemical Methods*, John Wiley & Sons, New York, 1980.
41 S. Song, X. Wang and P. Xiao, *Mater. Sci. Eng., B*, 2002, **94**, 40–47.
42 N. Naseri, H. Kim, W. Choi and A. Z. Moshfegh, *Int. J. Hydrogen Energy*, 2012, **37**, 3056–3065.
43 H. Wang, J. He, G. Boschloo, H. Lindstrom, A. Hagfeldt and S. E. Lindquist, *J. Phys. Chem. B*, 2001, **105**, 2529–2533.